COMPARISON OF SATELLITE BASED CLOUD RETRIEVAL METHODS FOR CIRRUS AND STRATOCUMULUS

Lindsay Parker
Aerospace Technologies Division, Planning Research Corporation
Hampton, VA. 23666

Bruce A. Wielicki
Atmospheric Sciences Division, NASA Langley Research Center
Hampton, VA. 23665-5225

1. INTRODUCTION

One difficulty in using satellite remote sensing data is the spatial variability of cloud properties on scales smaller than most meteorological satellite fields of view (approximately 4 to 8 km). The present study examines the variation of satellite derived cloud cover as a function of the satellite sensor spatial resolution for seven cloud cover retrieval methods:

1.	**Reflectance Threshold**:	Threshold = clear-sky reflectance Rclr + 3%
2.	**Temperature Threshold**:	Threshold = clear-sky temperature Tclr - 3K
3.	**ISCCP**:	Bispectral threshold (Rclr + 3% , Tclr - 3K)
4.	**HBTM**:	Hybrid Bispectral Threshold Method (Minnis et al., 1987)
5.	**NCLE**:	Bispectral method (Stowe et al., 1988)
6.	**Spatial Coherence**:	Coakley and Bretherton (1982)
7.	**Functional Box Counting**:	Lovejoy et al. (1987)

The first two methods are simple mono-spectral thresholds which specify a satellite pixel as cloud filled if the measured reflectance is greater than the threshold, or if the measured equivalent blackbody temperature is less than the threshold.

The next three methods are bispectral, using one visible wavelength window channel and one thermal infrared wavelength window channel. For ISCCP, the pixel is classified as cloud filled if the measurement exceeds either one of the single spectral channel thresholds. The HBTM has a more complicated strategy explained in Minnis and Harrison (1984) and Minnis et al (1987). One of the critical features of the HBTM is a series of checks of retrieved cloud albedo against climatological values. The NCLE yields a weighted cloud cover from two independent estimates of total cloud cover (one from an infrared channel at $11.5\mu m$ and one from a UV channel at $0.38\mu m$). The philosophy of the NCLE is to use the TOMS reflectance channel for boundary layer clouds (i.e. low thermal contrast) and to use the THIR 11.5 μm channel for middle and high level clouds (i.e. strong thermal contrast) as detailed in Stowe et al(1988).

The final two algorithms rely on the spatial variability within the cloud field to determine cloud cover. Spatial coherence assumes only that the cloud field occurs in a single layer and that the clouds are optically thick in the infrared window. Functional box counting uses the variation in reflectance threshold cloud cover over spatial scales observed by the satellite (here assumed to be 1 to 8 km for meteorological satellites) to predict the cloud cover for scales smaller than those observed (less than 1 km). This method relies on spatial scale invariance of the radiance fields to account for the resolution dependence of cloud cover. The study of Lovejoy et al (1986) used radar and GOES satellite data to indicate that this scale invariance held to scales in the atmosphere as small as 1 km.

Landsat Thematic Mapper (TM) data is used to test the spatial resolution dependence of the cloud algorithms. The TM radiometer has a near visible channel at $0.83\mu m$ and a thermal infrared window channel at $11.5\mu m$. The spatial resolution of the visible channel is 28.5 meters and the infrared channel is 114 meters. The full resolution data for these two spectral bands is then averaged in steps of two to provide spatial resolutions of 28.5m, 57m, 114m, 228m, 456m,

912m, 1824m, 3648m, and 7296m. These spatial resolutions are referred to in the following discussions as nominally 1/32, 1/16, 1/8, 1/4, 1/2, 1, 2, 4, and 8 km resolution data.

The ISCCP bispectral threshold applied to the full resolution data is used as the reference or "truth" cloud cover, after which the retrieval methods are applied to each of the spatial resolutions. For most of the scenes, sufficient clear regions are present in the full resolution Landsat data to use the peak of the bispectral histogram to define Rclr and Tclr. In the remaining scenes, the cloud field images were examined to select radiances in clear regions between cloud cells (at least 0.5 km from the nearest cloud cell). The same Rclr and Tclr are used at all spatial resolutions, for all retrieval methods, with the exception of the spatial coherence method which calculates its own clear and cloudy radiances. Note that reflectance is defined by $R = 100 \pi L / (S(t) \cos\theta_s)$ where L is spectral radiance derived using the calibration coefficients of Markham and Barker (1986), S(t) is the spectral solar constant for the date of the observation and θ_s is the solar zenith angle. Brightness temperature calibration for the thermal channel is also taken from Markham and Barker (1986). The Landsat viewing angles are within 5 degrees of nadir.

Studies of the fraction of pixels in the scene at cloud edge, and of the profile of reflectance and temperature near cloud edges indicate an uncertainty in the reference cloud fraction of 1 to 5% (Minnis and Wielicki, 1988).

2. RESULTS

The 24 cloud regions are 58.4 km by 58.4 km and are grouped and analyzed by cloud type (cirrus, cumulus, etc). Table 1 gives the location, date, reference cloud fraction, clear-sky brightness temperature (Tclr), clear-sky reflectance (Rclr), average cloudy pixel temperature (Tcld), average cloudy pixel reflectance (Rcld), and a description of the cloud types present. The descriptions are based on examination of the full resolution visible and infrared cloud images, and the bispectral histograms of the cloud fields. The cloud top temperatures given in the description are taken from the optically thick portions of the cloud fields as identified in the bispectral histograms (i.e. nadir reflectance greater than 40%). Where two distinct cloud levels occurred, both cloud tops are given. Time of observation for the Landsat sun-synchronous orbit is approximately 9:45 a.m. local time.

TABLE 1. CLOUD FIELD LOCATIONS, TIMES, AND PROPERTIES

Scene	Lat/Lon	Date Da/Mo/Yr	Cloud Cover	Rclr (%)	Rcld (%)	Tclr (K)	Tcld (K)	Description (Cld top temp)
A	19.7S/ 75.3W	7/13/87	0.671	2.5	19.5	289.7	287.5	Stratocumulus (285K)
B	20.7S/ 75.1W	7/13/87	0.915	2.5	28.2	289.7	286.5	Stratocumulus (284K)
C	33.7N/129.9W	7/10/87	0.521	3.3	21.4	288.8	285.6	Stratocumulus (283K)
D	26.4N/ 79.4W	1/14/83	0.708	4.0	44.6	298.0	280.5	Stratocumulus (272K)
E	25.7N/ 78.3W	1/14/83	0.390	3.5	52.4	296.3	277.4	Stratocumulus (270K)
F	31.8N/122.2W	7/07/87	0.662	3.8	33.3	289.7	284.8	Stratocumulus (283K)
G	31.8N/120.7W	6/30/87	0.889	2.7	38.7	288.8	282.9	Stratocumulus (282K)
H	28.3N/ 90.0W	1/06/83	0.718	3.2	11.8	305.4	279.2	Cirrus (≈220K)
I	44.6N/ 86.9W	10/28/86	0.950	4.3	13.8	280.5	266.5	Cirrus (≈243K,≈220K)
J	43.0N/ 87.5W	10/28/86	0.646	3.6	9.1	283.5	273.9	Cirrus (≈238K)
K	40.3N/ 71.8W	4/19/85	0.568	4.1	6.2	276.9	269.1	Cirrus (≈264K,≈254K)
L	40.3N/ 70.3W	5/30/85	0.839	5.3	8.6	278.5	270.5	Cirrus (≈262K)
M	28.9N/ 87.6W	3/15/84	0.625	3.5	14.9	287.8	273.1	Cirrus (≈254K)

a. Stratocumulus Cloud Fields

Results for stratocumulus are given in Fig. 1 (Scenes A-G, Table 1). The Reflectance, ISCCP and HBTM methods are within 0.05 of cloud "truth" for spatial resolutions less than 1/2 kilometer. These methods show a strong dependence on spatial resolution for pixel sizes beyond 1/2 kilometer. The Reflectance and ISCCP methods overestimate cloud fraction by 0.16 and the

HBTM by 0.09 for 8 kilometer data. The overestimation of cloud fraction is caused by partially filled pixels being considered as cloud filled pixels.

The Temperature threshold method underestimates cloud cover by about 0.20 at all spatial resolutions. Comparing the ISCCP bispectral result to the Reflectance and Temperature threshold results, we conclude that the solar reflectance channel dominates the bispectral cloud retrieval for stratocumulus. While this result is qualitatively expected, the magnitude of the difference in cloud cover (0.35) between the mono-spectral threshold methods is surprising. Examining Table 1, three of the stratocumulus cloud fields have T_{clr} - T_{cld} of 2.2 to 3.2K. These same three cases also have the lowest cloud reflectances, ranging from 19.5 to 28.2%. The low reflectances indicate that substantial portions of the cloud field have 11.5μm emittances less than 1.0. In this case, substantial portions of the cloud field are missed by the T_{clr} - 3K threshold. These optically thin portions of the cloud fields are also the cause of the underestimate of cloud cover by 0.12 for the Spatial Coherence results in Fig. 1. The Spatial Coherence method derives an effective cloud cover which is cloud fraction times cloud emittance.

For low clouds the NCLE algorithm gives strongest weighting to the cloud cover derived using the reflectance of the TOMS 0.38μm channel. Therefore, we would expect good results for the stratocumulus clouds. Fig. 1, however, indicates that the NCLE underestimates the cloud fraction by about 0.20. The NCLE algorithm determines its TOMS-based cloud cover as a linear function of reflectance between the clear reflectance and an assumed overcast cloud albedo of 50%. In the present analysis, Landsat nadir reflectance is substituted for albedo using the Earth Radiation Budget Experiment (ERBE) anisotropic models for overcast cloud (Suttles et al, 1988) to convert albedo to an equivalent nadir reflectance. This gives an overcast nadir reflectance of 51%, 48%, and 45% for solar zenith angles of 32°, 41°, and 49° respectively. The average stratocumulus nadir reflectance in Table 1, however, is only 34.0%. As a result, the NCLE algorithm underestimates the cloud fraction for these cloud cases. The NCLE albedo for overcast low cloud was derived by averaging the 0.38μm reflectance of TOMS fields of view (45 km at nadir) judged to be cloud filled (L. Stowe, personal communication). An examination of the Landsat spatially degraded data showed that the albedo of cloud filled pixels is a systematic function of pixel size. The average reflectance of 1/32 km pixels is 34.0%, 1/8 km is 37.0%, 1/2 km is 42.3%, and 2 km is 47.0%. For 8 km pixels, only cloud fields D-G have overcast pixels, with an average reflectance of 58.1%. We conclude that the larger the spatial extent of the contiguous cloud cover, the larger the cloud optical depth. This brings into question the NCLE assumption of cloud cover linear in cloud reflectance. A caveat on this result, however, is the use of the Landsat 0.83μm Landsat channel to mimic the 0.38μm TOMS channel.

Finally, Fig. 1 shows that the Functional Box counting method underestimates cloud fraction for spatial resolution less than 1 kilometer. This method assumes the slope of the change in cloud cover from 1 to 8 km can be extended to scales less than 1 km. Fig. 1 demonstrates this method is incorrect. Cahalan (1988) and Welch et al (1989) found a break in the scale invariance between 0.5 and 1.0 km, consistent with the present results.

Fig. 2 gives a scatter plot of the estimated versus reference cloud fraction for each retrieval method. This figure demonstrates that the mean errors examined in Fig. 1 vary greatly from cloud field to cloud field.

Fig. 3 gives the Temperature, Reflectance, and ISCCP Bispectral thresholds which would result in unbiased cloud cover estimates for the seven stratocumulus cloud fields. As spatial resolution degrades, the reflectance and ISCCP thresholds must be further removed from the clear-sky background to avoid the biasing effect of partially cloudy pixels. ISCCP and the Reflectance threshold would require a threshold of 9.5% for stratocumulus clouds using 8km spatial resolution data. The Temperature threshold would require a threshold of T_{clr} - 1.5K colder than the clear-sky temperature. Unfortunately, use of temperature thresholds much less than T_{clr} - 3K would cause false detection of cloud given typical variations in ocean surface temperature and atmospheric water vapor.

b. Cirrus Cloud Fields

Results for cirrus are given in Fig. 4 (Scenes H-M Table 1). The results for cirrus are very different from the stratocumulus results. The cirrus results show little dependence on the sensor spatial resolution, indicating that the cirrus are not dominated by the small scale cellular features prevalent in the stratocumulus fields. The effect of spatial resolution on derived cloud cover is less than 0.02 for spatial scales less than 2 km, reaching 0.07 for the ISCCP algorithm using 8 km resolution data.

The agreement between the Temperature threshold and ISCCP bi-spectral results indicates the dominance of the 11.5μm channel for cloud detection of cirrus. Consistent with this view, the Reflectance threshold underestimates cirrus cloud cover by 0.18 to 0.25, depending on the spatial resolution. The cirrus clouds are optically thin with an average Rcld of 10.6%. As a result, the Reflectance threshold misses a substantial portion of the cloud field with reflectances less than 3% above the clear reflectance. The HBTM results are intermediate between the Reflectance and Temperature threshold results, underestimating cirrus cloud cover by 0.10 for 8 km resolution data.

The cloud cover underestimate by the Spatial Coherence method is larger than that found for stratocumulus because the cirrus emittance is lower. The Box Counting method underestimates cirrus cloud cover for two reasons. First, the reflectance threshold causes an underestimate as discussed above. Second, the scale invariance is again a poor approximation for spatial scales less than 1 km. For these cirrus clouds, the scale invariance appears to be a poor approximation even for scales of 1 to 8 km, in contrast to the result for stratocumulus cloud fields.

Finally, the NCLE result underestimates cirrus cloud cover by 0.38 to 0.42. This result appears to be caused by two factors. First, the NCLE uses a Tclr - 6K threshold at 11.5μm, thereby missing some of the cirrus detected by the ISCCP method using a Tclr - 3K threshold. This was especially important for cloud fields K and L for which the average Tcld was only 7 to 8 K colder than Tclr. A second difficulty is that the TOMS reflectance channel cloud cover estimate is still being given significant weight by the NCLE algorithm. This is because much of the cirrus cloud field is warmer than the approximately Tclr - 9K temperature used to separate low level from middle and high level clouds. These "warm" portions of the cloud field are treated as if they were low cloud, thereby using the TOMS channel cloud estimate. Since the cirrus reflectance is much less than 50%, the TOMS channel greatly underestimates the cirrus cloud cover.

Figure 5 gives the estimated versus reference cloud cover results for each individual cloud field. As for stratocumulus, the errors are not a simple constant bias. Figure 6 gives the threshold levels which if applied to the 6 cirrus fields would have resulted in an unbiased cloud cover. The thresholds show less dependence on spatial resolution than was found for the stratocumulus cloud cases.

3.   SUMMARY

1. For the threshold methods, stratocumulus cloud cover is strongly dependent on satellite sensor spatial resolution. Cirrus cloud cover is weakly dependent on satellite sensor spatial resolution.

2. Differences between current cloud retrieval algorithms are large, especially between the ISCCP and NCLE algorithms.

3. Varying treatment of cloud optical thickness (i.e. shortwave reflectance or thermal emittance) appears to account for many of the differences in the cloud retrieval algorithms.

4. Functional Box Counting incorrectly estimates cloud fraction below 1 km due to breaks in the scale invariant power law between 0.5 and 1 km for stratocumulus and 2-4 km for cirrus.

5. For the threshold cloud retrieval methods, the solar reflectance channel dominates cloud cover retrieval for stratocumulus, while the thermal channel dominates for cirrus.

REFERENCES

Cahalan, R. F., 1988: in Scaling, Fractals, and Nonlinear Variability in Geophysics, Ed. S. Lovejoy and D. Schertzer.
Coakley, J. A. and F. P. Bretherton, 1982: JGR, 87, 4917-4932.
Lovejoy, S. et al, 1987: Science, 235, 1036-1038.
Markham, B. L. and J. L. Barker, 1986, Landsat Technical Notes, Aug. 1986.
Minnis, P., E. F. Harrison, and G. G. Gibson, 1987:, J. Geophys. Res., 92, 4051-4073.
Minnis P. and B. A. Wielicki, 1988: JGR, 93, 9385-9403.
Platt, C. M R. et al, 1980: MWR, 108, 195-204.
Stowe, L. L. et al., 1988: J. Clim., 1, 445-470.
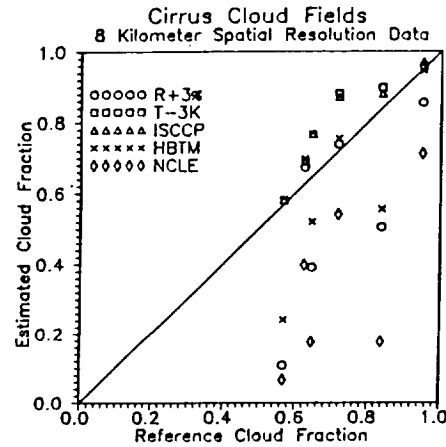Welch, R. M. et al., 1988: JAM, 27, 341-362.

Fig. 1

Fig. 2

Fig. 3

Fig. 4

Fig. 5

Fig. 6